



Micro milling of different workpiece materials with all-ceramic Y-TZP and cemented carbide micro end mills

Tobias Mayer¹ · Sonja Kieren-Ehse¹ · Benjamin Kirsch¹ · Jan C. Aurich¹

Received: 26 October 2023 / Accepted: 9 January 2024
© The Author(s) 2024

Abstract

Micro milling is a very flexible micro cutting process widely deployed to manufacture miniaturized parts. However, size effects occur when downscaling the cutting processes. They lead to higher mechanical loads on the tools and therefore increased tool wear. Micro milling tools are usually made of cemented carbides due to their mechanical strength and fine grain structure. Technical ceramics as alternative tool materials offer very good mechanical properties as well, with grain sizes well below 1 μm . In conventional machining, they have proven to be able to reduce tool wear. To transfer these wear improvements to the micro scale, we manufactured all-ceramic micro end mills in previous studies (\varnothing 50 and \varnothing 100 μm). Tools made from zirconia (Y-TZP) showed the sharpest cutting edges, and were the best performing in micro milling trials amongst the substrates tested. However, the advantages of the ceramic substrate could not be utilized for the brass and titanium materials tested in those studies. Therefore, in this study the capabilities of all-ceramic micro end mills (\varnothing 50 μm) in different workpiece materials (1.4404, 1.7225, 3.1325 and PMMA GS) were researched. For the two steels and the aluminum alloy, the ceramic tools did not offer an improvement over the cemented carbide tools used as reference. For the thermoplastic PMMA however, significant improvements could be achieved by utilizing the Y-TZP ceramic tools: Less tool wear, less and more stable cutting forces, and higher surface qualities.

Keywords Micro milling · All-ceramic end mills · Ultra small micro end mills · Ceramic tool substrates · Tool development · Tool wear

1 Introduction

Micro milling as a cutting process is widely deployed in many different sectors to manufacture miniaturized parts such as micro pumps or turbines for micro reactors [1], microlenses or lens arrays for image sensors, micro molds and dies in micro injection molding, and many more [2]. Micro milling is very flexible in terms of machinable workpiece materials and geometries [3], and is generally defined as a downscaled conventional milling process with tool diameters below 1 mm [4]. With decreasing tool diameters, however, simply downscaling the parameters from conventional milling is not possible due to the occurring size effects. Size effects are deviations from proportional

values, or ratios thereof, that occur when scaling geometric dimensions [5]. The ratio of the uncut chip thickness to cutting edge radius is a dominant size effect in micro milling, as the cutting edge sharpness is limited by the tool substrates and their manufacturing processes, and cannot be decreased proportionally [6]. As the ratio decreases, the process behavior becomes more and more different from conventional cutting, for which the cutting edge is usually assumed as ideally sharp. Low ratios result in a large degree of ploughing when the minimum chip thickness cannot be reached, and high specific cutting forces due to the increased amount of friction. These in turn lead to high tool wear and a low surface quality [7]. With decreasing tool diameters this becomes even more pronounced, since the tool's stiffness decreases with the diameter. Tool deflections thus can reduce the achievable parts accuracy, and tool breakages are much more likely to occur than in conventional machining [8]. Additionally, with low tool diameters and uncut chip thicknesses, the workpiece materials generally cannot be viewed as homogenous anymore. The cutting process takes

✉ Tobias Mayer
tobias.mayer@rptu.de

¹ Institute for Manufacturing Technology and Production Systems, RPTU Kaiserslautern, Gottlieb-Daimler-Str., 67663 Kaiserslautern, Germany

place inside individual grains instead of the bulk material, which can lead to rapidly changing material properties due to different grain orientations [9].

Overall, the size effects result in high specific cutting forces the micro tools need to be able to withstand, and also result in increased wear and lower structure quality and parts precision. Therefore, micro milling tools are usually made of cemented carbide due to their very good mechanical properties [10], as well as their low grain sizes of down to $0.2\ \mu\text{m}$ [11]. This allows the cutting edge radius of the manufactured tools to be in the range of $0.1\text{--}0.3\ \mu\text{m}$ [12], resulting in a very low minimum chip thickness, as that is directly linked to the cutting edge radius [13]. Based on most experimental and simulation results in literature, it can be said that the minimum uncut chip thickness usually lies in the range of 20–40% of the cutting edge radius [14]. Thus, lower uncut chip thicknesses can be used without introducing ploughing, and a better surface roughness be generated [6]. Most micro tools are manufactured via grinding processes. These are advantageous due to the achievable quality and geometry, as well as their high material removal rates [15]. With smaller tool diameters, downscaling the geometry from macro processes leads to weak cross sections, low tool strength and frequent tool failure. The tool geometry in micro processes thus needs to be adapted to achieve robust stiffness and mechanical strength [16]. For ultra small micro end mills with diameters below $50\ \mu\text{m}$, asymmetric single fluted designs such as the D-shape used in this study are common [17].

Technical ceramics as an alternative tool material offer very good mechanical properties as well, especially concerning hardness at elevated temperatures and chemical inertness. In addition, grain sizes well below $1\ \mu\text{m}$ are available for certain fully dense ceramics [18]. Most ceramic tools in conventional machining are ceramic inserts [19], while for solid, all-ceramic milling tools only few publications can be found. The available studies, however, show that these often perform better than cemented carbides when machining difficult-to-cut workpiece materials: Uhlmann and Hübert e.g. developed full-body ceramic end mills ground from whisker reinforced alumina and silicon nitride, which outperformed coated cemented carbide tools in high-speed milling of Inconel 718 [20]. Finkeldei et al. were able to increase performance in machining of Inconel 718 with silicon nitride ceramic end mills over cemented carbide tools as well [21]. Wang and Liu utilized silicon nitride and cermet end mills to reduce tool wear and cutting forces when machining hardened AISI H13 steel (60–62 HRC) with increased surface quality [22].

However, the literature mostly covers tool sizes from 1–2 mm in diameter and up. We wanted to investigate whether it was possible to transfer the beneficial wear behavior shown in conventional milling down to the micro

scale. Therefore, in our investigations we manufactured micro end mills with diameters of $100\ \mu\text{m}$ and below. We could show that it is possible to manufacture all-ceramic micro end mills with $50\ \mu\text{m}$ diameter via grinding. Wheel dressing and minimum quantity lubrication are needed to ensure a stable manufacturing process, as the ceramic tool blanks result in higher grinding wheel wear compared to cemented carbide tools. We manufactured tools from four different ceramics (alumina, zirconia toughened alumina—ZTA, yttria stabilized tetragonal zirconia polycrystal—Y-TZP, and silicon nitride). Our research showed that the tools made from Y-TZP were not only the sharpest all-ceramic tools, but that they were the best performing in micro milling trials as well. Out of the four ceramic tool substrates tested, the Y-TZP micro tools were the only ones that did not suffer catastrophic tool failures; however, they exhibited a high amount of tool wear. Overall, the Y-TZP ceramic was the most promising ceramic tool substrate with the sharpest cutting edge radii, the best structure quality, a predictable wear behavior and no tool breakages. Therefore, it was deemed to be the best candidate for all-ceramic micro end mills for further investigations [23].

The different behavior of zirconia versus the other substrates can be explained by its martensitic phase transition from the tetragonal to the monoclinic phase. This acts as a transformation toughening mechanism, which leads to an increase in fracture toughness [24]. The stress at the tip of a crack can initiate a phase transformation: The increase in volume from the lattice change and the formation of a ‘transformation zone’ around the crack can then slow down its growth or even stop it completely [25]. For pure zirconia, the transition to the tetragonal phase happens at around $1000\ ^\circ\text{C}$. To benefit from the abovementioned transition toughening, the tetragonal phase needs to be stabilized so that it is present at normal temperatures. This is usually done through the addition of yttria, which yields yttria stabilized tetragonal zirconia polycrystal (Y-TZP). In general, alloying amounts of 3 mol% Y_2O_3 are used, which also results in very fine grain structures [26] advantageous to the micro end mill grinding process [6].

In our previous investigation, we deployed the all-ceramic micro end mills in brass and commercially pure titanium grade 2 (Ti2). Smooth micro milled structures were achieved in brass without tool wear, which can be done with most tool substrates available, though. For Ti2, severe abrasive wear not present for cemented carbide tools was ascertained, making machining of Ti2 unfeasible [23]. The advantages of the ceramic substrates thus could not be utilized for those workpiece materials. Therefore, the present study researches the capabilities of all-ceramic micro end mills in different workpiece materials: A

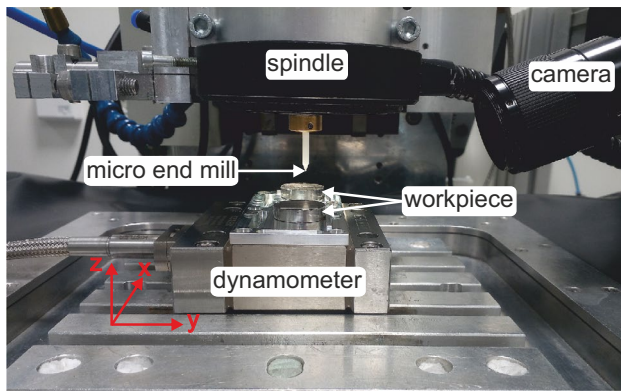


Fig. 1 High precision CNC 3-axis machine tool used for the micro milling experiments

stainless steel and a tempering steel, an aluminum alloy, and a thermoplastic.

2 Materials and methods

2.1 Machine tools, tooling, and workpiece materials

The micro milling experiments in this study were performed on a high precision CNC 3-axis machine tool developed at our institute, see Fig. 1.

The machine tool has a granite base that is vibration isolated via pneumatic dampers. The X- and Y-axes are stacked and air bearing operated. They are ball screw driven via stepper motors, with a total travel range of 100 mm. The smallest movement increment is 20 nm, and the two-sided positioning accuracy is below 1.5 μm . The vertical Z-Axis utilizes cross-roller bearings to support the weight of the machining spindle, with otherwise similar specifications. The main spindle is a Westwind¹ type L3578 air bearing spindle, capable of speeds up to 50,000 rpm. The dynamic runout at the tool tip is below 1.8 μm over the entire speed range. This is in the same order of dimension as the chip thickness: The tools could possibly be damaged if the runout at the backside (flank face and onward) of the tool were larger than their clearance. Therefore, a safety factor is added to the maximum clearance during tool grinding. In addition, the runout directly affects the actual chip thickness and slot width during cutting by either increasing or decreasing it. This is dependent on the angular relation between synchronous runout and the tool's cutting edge, and varies for each revolution with the asynchronous portion of the runout. Process monitoring and optically setting the Z-coordinate of the workpiece surface via touching was done with a Navitar¹ 12 \times Zoom camera system with a 2MP CMOS chip. The touching accuracy, and thus the position

of the workpiece surface, is usually within 0.5 μm . The workpieces were glued onto a sample holder, which was then screwed onto a dynamometer used in all experiments to measure the cutting forces.

The all-ceramic tools used in the micro milling experiments were made from Y-TZP, and the micro end mills used as references from WC/Co cemented carbide. Table 1 shows the properties of the tool blanks (\varnothing 3 mm h6 \times 39 mm), as supplied by Situs Technicals¹ and Hyperion¹.

The tools were ground on an LT Ultra¹ MTC 250 ultra-precision lathe. The customized grinding setup consists of a rough and fine grinding wheel (#800 and #4800) with a hydrodynamic spindle and an air turbine spindle to grind the rough and fine tool geometry, respectively. The tool geometry is produced by linear motions, resulting in the facets visible in Fig. 2. For further information on the tool grinding process and the grinding setup we refer to [27]. The tools featured a single edged geometry [27] with zero-degree helix and rake angle, and were 50 μm in diameter. The tool geometry is shown in Fig. 2.

Since ceramic substrates in conventional machining usually excel at cutting hard to machine materials, two different steels were chosen: The stainless steel 1.4404, which results in high tool wear when micro milling [28], and 1.7225 (quenched and tempered) as a commonly used tempering steel. Due to the high tool wear we saw in our previous investigations during machining of Ti2, two softer and easier to machine materials were included in this study as well: The aluminum alloy 3.1325, commonly used as a higher strength aluminum alloy, and the thermoplastic polymethylmethacrylate (PMMA GS) which results in high flank wear when micro milling with cemented carbide tools [29]. Table 2 shows the properties of the workpiece materials.

Table 1 Mechanical properties of the ceramic tool substrate and the cemented carbide used as reference tool substrate

		Situs Technicals 3Y-TZP	Hyperion PN90 (WC/ Co)
Density	g/cm^3	6.05	14.55
Cobalt/yttria content	wt%	5.1	9
Grain size	μm	0.5	0.2
Rockwell hardness		78 HR-45N	93.9 HRA
Transversive rupture strength	MPa	1200	4700
Fracture toughness	$\text{MPam}^{1/2}$	8	7.8

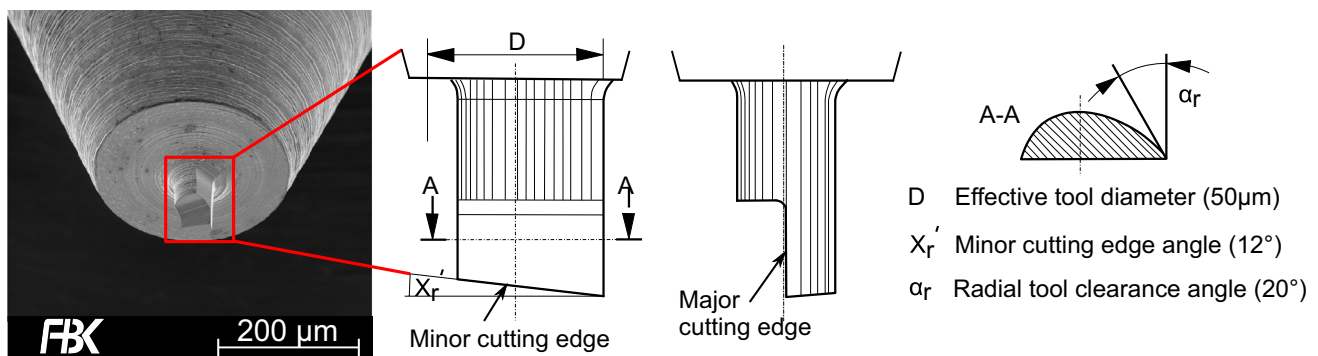


Fig. 2 Geometry and parameters of the micro end mills used in this study, illustration after [27]

Table 2 Mechanical properties of the four different workpiece materials

		1.7225	1.4404	3.1325	PMMA GS
Young's modulus	GPa	210	193	70	1.8–3.1
Tensile strength	MPa	1000–2000	485	390	48–76
Yield strength	MPa	750	170	245	–
Hardness	HB	350	217	110	–
Thermal conductivity	W/mK	40–45	15	130–200	0.2

Table 3 Parameters of the micro milling experiments

Machining conditions	Spindle speed	30,000 rpm
	Feed per tooth	1.2 µm
	Depth of cut	5 µm (2 µm for 1.4404)
	Feed travel	1.3 m (0.9 m for 1.4404)
Micro end mills	Tool substrates	3Y-TZP Cemented carbide
	Tool diameter	50 µm
	Rake angle	0°
Workpiece materials	Helix angle	0°
	Stainless steel	1.4404
	Tempering steel	1.7225
	Aluminum alloy	3.1325
	Thermoplastic	PMMA GS

2.2 Experimental setup and cutting parameters

Prior to the micro milling experiments, the workpieces were face milled with a $\varnothing 3$ mm end mill. The spindle was kept running for a minimum of 10 min before the micro milling experiments to reach a thermal equilibrium, and to avoid temperature related changes in the cutting depth. The cutting parameters were held constant for all experiments conducted: A spindle speed of 30,000 rpm was used, with a feed per tooth of 1.2 µm and a depth of cut of 5 µm. The depth of cut had to be adjusted down to 2 µm for the micro milling experiments in 1.4404 with the all-ceramic micro end mills, as these did suffer from near immediate tool breakages otherwise. The feed travel was realized with 20 mm long meandering slots over a total length of 1300 mm. Due to the sample size, only 900 mm of feed travel could be realized on the 1.4404 samples. As the tool wear for the all-ceramic end mills occurred in the first 200 mm of feed travel, this was deemed acceptable. The number of slots and their length were adjusted to the sample geometry in such a way that the entire feed travel was continuous, with the tool never leaving the workpiece. A summary of all experimental parameters is shown in Table 3. For all four workpiece materials, three experiments were conducted with all-ceramic micro end mills, plus a reference cut with a cemented carbide tool.

2.3 Measurement technology and data analysis

The micro end mills were imaged via scanning electron microscopy (SEM). Their cutting edge topography was measured via atomic force microscopy (AFM) before and after the micro milling experiments. For the SEM imaging, the tools were cleaned in an ultrasonic bath with isopropyl alcohol, and the scanning parameters for the FEI¹ Quanta 600 FEG microscope used were as follows: Working distance 10 mm, acceleration voltages 5 kV and 20 kV for the all-ceramic and cemented carbide tools, respectively. The micro milled structures were imaged after the experiments using the same process, with the PMMA samples being gold sputtered before imaging, also.

The characterization of the tools' cutting edge topography was done with a Nanosurf¹ NaniteAFM that is integrated into another desktop sized machine tool at our institute. A 30 µm × 15 µm area of the cutting edge of each tool was measured. From the measured topographies, the cutting edge radius can then be calculated for each cross section and the entire cutting edge, see [12] for further information.

Combined with the SEM images, this allows for both a qualitative and a quantitative analysis of the tools.

During the micro milling experiments, the cutting forces were measured with the multi-component dynamometer (Kistler¹ type 9119AA1) mounted between the machining table and the sample holder. The analog output signal was amplified with three Kistler¹ type 5011 charge amplifiers and then digitized via a National Instruments¹ USB 6210 digital analog quantifier (DAQ). Subsequent filtering and processing were carried out in the National Instruments¹ DIAdem software suite: A bandpass (8th order Bessel filter, 250 Hz – 3500 Hz passband) shuts out AC mains noise as well as distortions above the dynamometer’s resonant frequencies. The X-, Y- and Z-channels are each processed individually and were recorded at a sampling frequency of 12 kHz. To get the active cutting force, the channels in feed and feed normal directions were combined via vector addition. The effective active and passive (orthogonal to feed and feed normal directions) cutting forces were then calculated using a root mean square (RMS) average with a two-sided window size equivalent to 500 tool revolutions. Further analysis and visualization of the cutting force values was done in Mathworks¹ Matlab, including calculating the specific forces by dividing the effective forces with the cutting depth.

The topography of the bottom surface of the milled slot was measured with a Nanofocus¹ µsurf OEM confocal

microscope, which is integrated into the same machine tool as the AFM. The lens used was 60× with a numerical aperture of 0.9, resulting in a maximum lateral resolution of about 0.5 µm. The measurement area covered 260 µm × 260 m, and two measurements were stitched together for a total measured area of 260 µm × 500 µm. The data was further analyzed in Digital Surf¹ MountainsMap 7. Both profile and areal roughness parameters were extracted in the software. The average roughness value Ra was calculated along the center of the milled slot according to ISO 21920-2 [30]. The lowest standardized gaussian filter length of 80 µm is too large for the micro milled structures, which have a periodic surface structure with a spacing equal to the feed per tooth (1.2 µm). By extrapolation of the values for periodic profiles and the cutoffs that were present in ISO 4288, a filter length of 8 µm was chosen [31]. Additionally, the average areal roughness Sa was calculated for an area of the length of the measurement area and 90% of the slot width as per ISO 25178-2 [32].

3 Results and discussion

3.1 Micro milling of 1.7225

Figure 3 shows one of the Y-TZP tools and the reference cemented carbide tool before and after deployment, as well

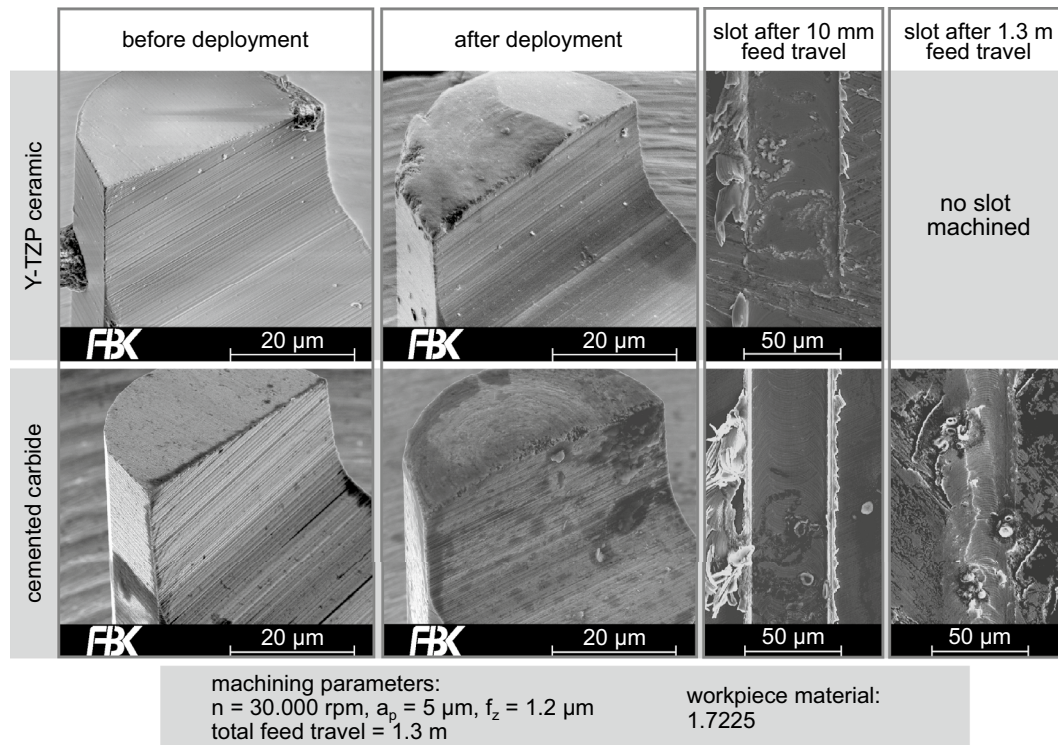


Fig. 3 Micro end mills and milled structures of the 1.7225 experiments

as the micro milled slots at the beginning and the end of the feed travel.

For the ceramic tool, a very large wear area can be identified on the flank face of the minor cutting edge. The micro milled slot at 10 mm feed travel is very shallow (about $1\ \mu\text{m}$). Also, it shows spots that were not actually machined and the previously face milled surface was not cut into. Alas, most of the tool wear had already occurred at this stage. The slots only get shallower from here, until no actual slot was milled anymore, and only ploughing and rubbing on the workpiece surface took place. After about 50 mm feed travel, no material removal was observed anymore. The second Y-TZP tool exhibited a near identical wear pattern and feed travel, while the third tool broke off shortly after workpiece contact.

The cemented carbide tool shows severe wear as well, however at a much higher feed travel. The tool did mill the entire feed travel, although like the ceramic tools, only ploughing occurred after about 100 mm feed travel. The milled slots were much deeper however, which can be seen comparing the slots of the ceramic tools and the cemented carbide tool at 10 mm feed travel, also. Thus, the wear occurred over a longer period rather than in the first few millimeters of feed travel. The wear pattern is more uniform, too: The flank face of the minor cutting edge is a planar surface, and a circular, smeared pattern is visible. The most wear occurred at the cutting edge corner so that the minor

cutting edge angle became negative, see Fig. 2 for the initial, correct geometry.

The wear patterns for both tool substrates suggests that a lot of material was ploughed and squeezed through beneath the minor flank face and the workpiece surface, which is confirmed by the SEM images of the micro milled slot bottoms. The measured cutting forces (not shown) show a similar trend as well: The active forces drop almost immediately after workpiece contact for the ceramic tools, while the passive forces rise. For the cemented carbide tool, the passive force rises a lot slower due to wear occurring later in the overall feed travel. For reference, the profile and areal roughness values after 10 mm of feed travel were $R_a = 21.7\ \text{nm}$ and $S_a = 47.1\ \text{nm}$ for the cemented carbide tool, and $R_a = 74.1\ \text{nm}$ and $S_a = 136.5\ \text{nm}$ for the ceramic tools (average over all 3), respectively. This again confirms the early onset of tool wear for the ceramic tools, which thus are not suitable to machine the 1.7225 material.

3.2 Micro milling of 1.4404

For the 1.4404 experiments, Fig. 4 depicts the micro end mills and the micro milled structures.

The overall result is similar to the 1.7225 experiments: The ceramic tools suffered severe wear at the minor cutting edge and only milled 30–50 mm of feed travel, while the cemented carbide tools suffered less wear and machined

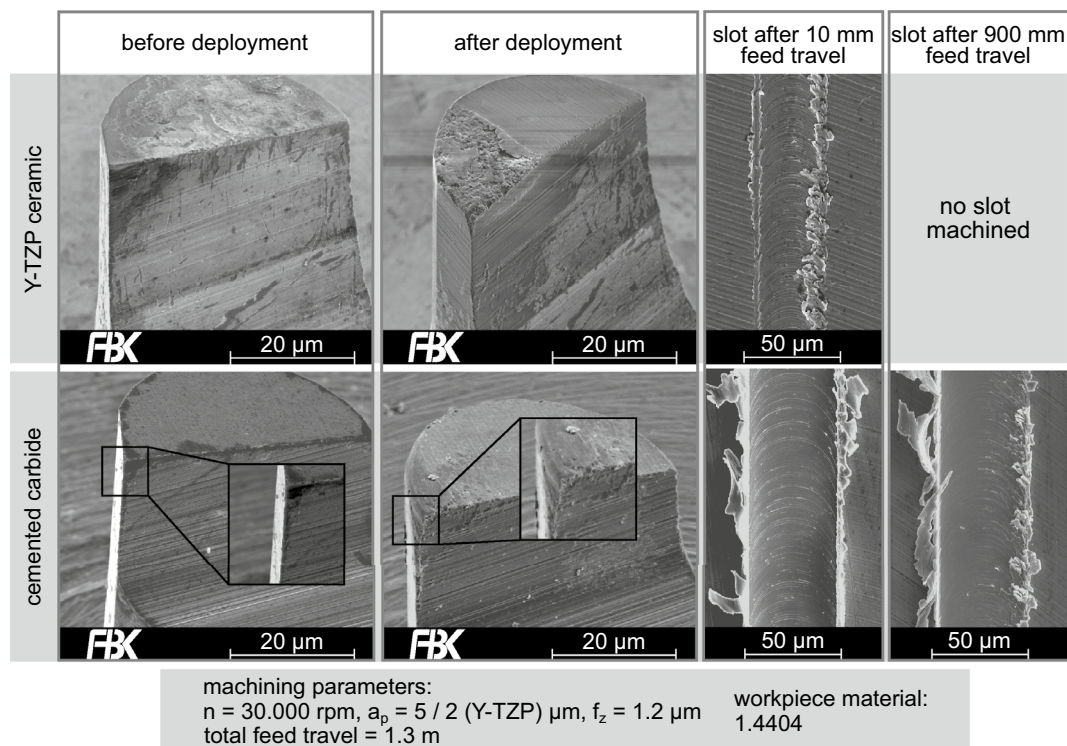


Fig. 4 Micro end mills and milled structures of the 1.4404 experiments

better structures. For the ceramic tools, the depth of cut had to be reduced from $5\ \mu\text{m}$ down to $2\ \mu\text{m}$. With the depth of cut of $5\ \mu\text{m}$, the tools suffered immediate failures after about 1–2 mm of feed travel. Even with the reduction, Fig. 4 shows the only ceramic tool that did not break off immediately in the experiments. As with the 1.7225 experiments, the tool wear appears on the flank face of the minor cutting edge. However, it appears as if pieces of the tool substrates were pulled out or broken away, suggesting adhesive rather than abrasive wear. Again similar to the 1.7225 experiments, the tool wear is apparent in the first slot after 10 mm of feed travel: The slot is very shallow (below $1\ \mu\text{m}$), there is a lot of smeared workpiece material especially on the right slot side, and the slot width is narrower than the effective tool diameter.

In contrast, the performance of the cemented carbide tool was much better for the stainless steel than for the tempering one: Tool wear is limited to a slight rounding of the cutting edges, and the slot bottom at the end of the feed travel shows only slight adhesions. The depth of cut did not need to be reduced as for the all-ceramic tools, either. Also, the profile and areal roughness values remained nearly the same, at $R_a = 36.2\ \text{nm}$ and $S_a = 72.2\ \text{nm}$ at a feed travel of 10 mm and $R_a = 23\ \text{nm}$ and $S_a = 83.2\ \text{nm}$ at a feed travel of 900 mm. Micro milling of 1.4404 is therefore feasible with cemented carbide tools, but not with the ceramic tools.

3.3 Micro milling of 3.1325

The results for the micro milling experiments in aluminum show less wear than for the two steels, as evident by the tools and slot bottoms in Fig. 5.

As can be seen in the SEM images of the tools after the experiments, the softer 3.1325 is prone to adhesions. This is visible in the milled slot bottoms, also, which show adhesions and smearing alike. Yet, even with the softer workpiece material, the ceramic tools exhibited a large amount of wear. Almost the entire rake and flank face show aluminum adhesions, and the cutting edge corner is severely rounded. This rounded corner stretches around about half the tool's backside, and has an approximate radius of $5\ \mu\text{m}$ (which corresponds to the depth of cut), occurring on all three Y-TZP tools used. Judging by the rounded corner and workpiece material adhesions on the tool, only few chips were formed during micro milling. Instead, the soft workpiece material squeezed through under the cutting edge corner, wearing the flank faces of the minor and major cutting edge alike. The slot at the end of the feed travel shows more material smeared across the slot bottom and at the side of the slot in comparison to the one at the start, also.

The workpiece material adhesions were significant for the cemented carbide tools as well, but either no tool wear occurred, or it was so small that the adhesions cover it. The quality of the micro milled slots is higher than for the

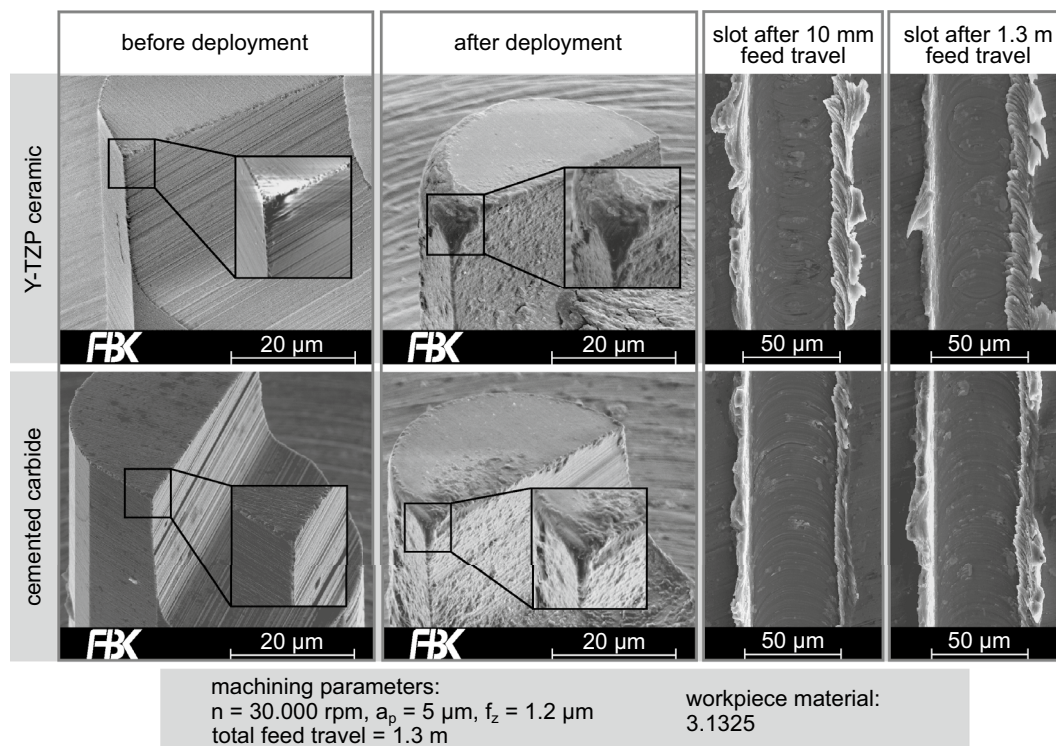


Fig. 5 Micro end mills and milled structures of the 3.1325 experiments

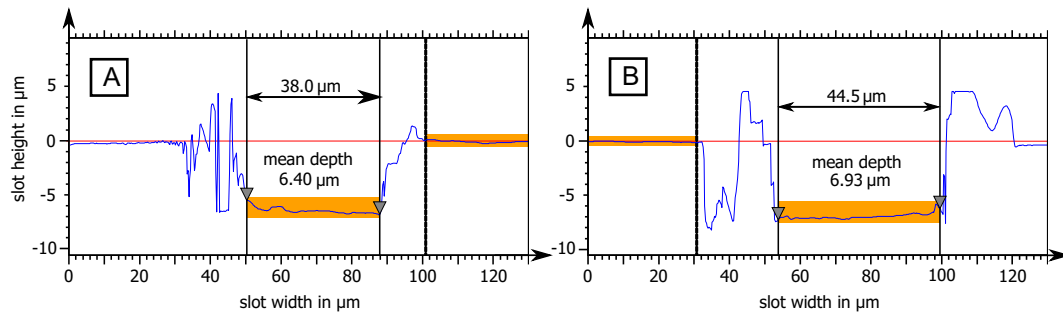


Fig. 6 Cross sections perpendicular to the feed direction of the micro milled slots in EN AW-2017A at about 1.3 m feed travel: **A** Y-TZP ceramic, **B** cemented carbide

Y-TZP tools. No visual difference in quality can be seen in the SEM images between the start and the end of the feed travel, either.

The difference in tool wear can be observed in the topography of the milled slots. A comparison between the slots milled with the Y-TZP ceramic and the cemented carbide tool is shown in Fig. 6, displaying cross sections of the last two slots at about 1.3 m feed travel each.

The effect of the rounded cutting edge corner of the ceramic tools can be easily identified: The sidewalls of the micro milled slots in Fig. 6A are skewed, and the resulting width of the slot bottom reduced. In comparison, the slots milled with the cemented carbide micro end mills in Fig. 6B feature almost vertical sidewalls, and a larger slot width at the bottom. The erratic height values to the left and right of the slots are measurement artefacts caused by the light diffraction of the burrs. The mean depth of the slots is similar for both tool substrates, but higher than the desired depth of cut. This could be explained by built-up edges and material squeezed under the minor cutting edge of the micro end mills, removing more material than the depth of cut set.

In addition to the topography discussed above, the specific cutting forces depicted in Fig. 7 show a rising tendency with increasing feed travel:

All tools show increasing active forces in Fig. 7A, with overall similar qualitative force curves. They are all in the same value range, except Y-TZP #1 which has an about 20% lower force level. This could be caused by a sharper cutting edge or a different tool clamping in relation to the runout (as described in Sect. 2). The active force for the cemented carbide tool stays constant until a feed travel of about 600 mm, after which it increases, too. For the passive forces in Fig. 7B the two tool substrates show different qualitative behaviors: While they start in the same range (except Y-TZP #1, again), the passive force for the cemented carbide tool stays almost constant, while for the ceramic tools they rise with increasing feed travel. This likely relates to increased ploughing due to the rounded part of the cutting edge corner. As the forces rise with increasing feed travel,

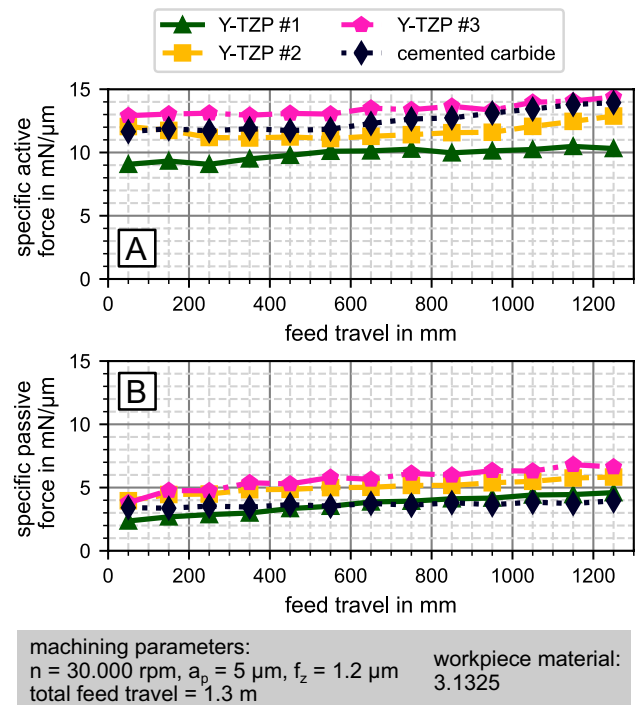


Fig. 7 Specific active (A) and passive (B) forces during micro milling of 3.1325, mean forces over 100 mm feed travel each, normalized with the slot depth as measured via confocal microscopy

it can be assumed that the wear development is somewhat linear as well.

The distinction between the two tool substrates is not as clear in the measured roughness values, see Fig. 8, however a trend is visible here as well.

For both the profile roughness R_a in A) as well as the areal roughness S_a in B), the cemented carbide tool achieved a constant low value without rising tendencies over the feed travel. Some variation can be observed for the R_a values, while the S_a values rise slightly in the first 200 mm of feed travel and are stable afterwards. The

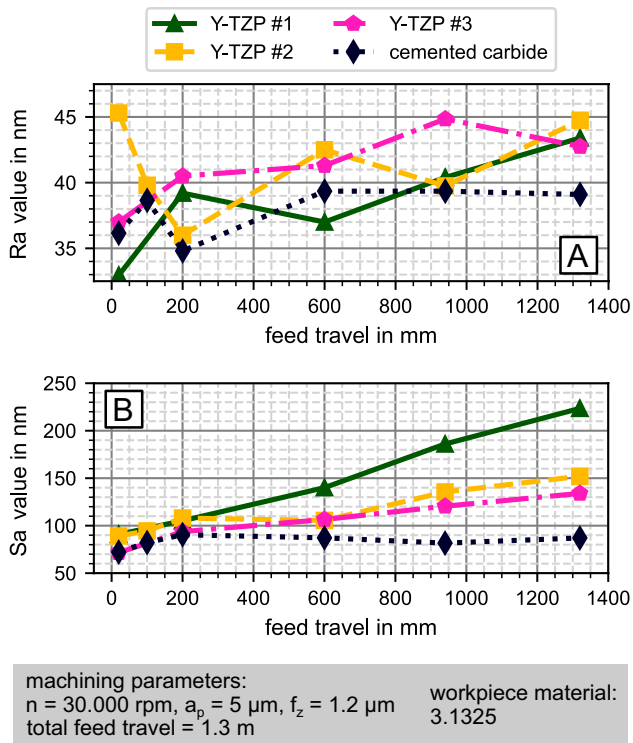


Fig. 8 Ra and Sa roughness values versus feed travel for the 3.1325 specimens

Y-TZP tools are in the same value range as the cemented carbide tool for Ra, although a trend towards increased Ra values at higher feed travels can be identified in Fig. 8A. The influence of the tool wear and the qualitative reduction in surface quality between the start and the end of the feed travel visible in Fig. 5 can be correlated to the Sa values in Fig. 8B. All ceramic tools show a strong increase in Sa over the feed travel, double of the initial value for tool #1 (which was an outlier for the process forces too), even. This again shows that the cemented carbide tools are the better choice for machining 3.1325. With the results presented, Y-TZP tools have no benefits versus cemented carbide ones when milling this aluminum alloy.

3.4 Micro milling of PMMA

In the micro milling experiments in PMMA, the cemented carbide tools exhibit a ‘wedge-like’ wear at the flank face, see Fig. 9.

This wear pattern is typical for deploying cemented carbide tools in PMMA, and hinders the manufacture of larger, high quality structures [29]. It is evident from the direct comparison of the tools from the two substrates in Fig. 9 that the wear situation has changed from the previous experiments: The ceramic tool shows significantly less tool wear, without the ‘wedge-like’ wear of the cemented carbide tool. Only a slightly rounded main cutting edge

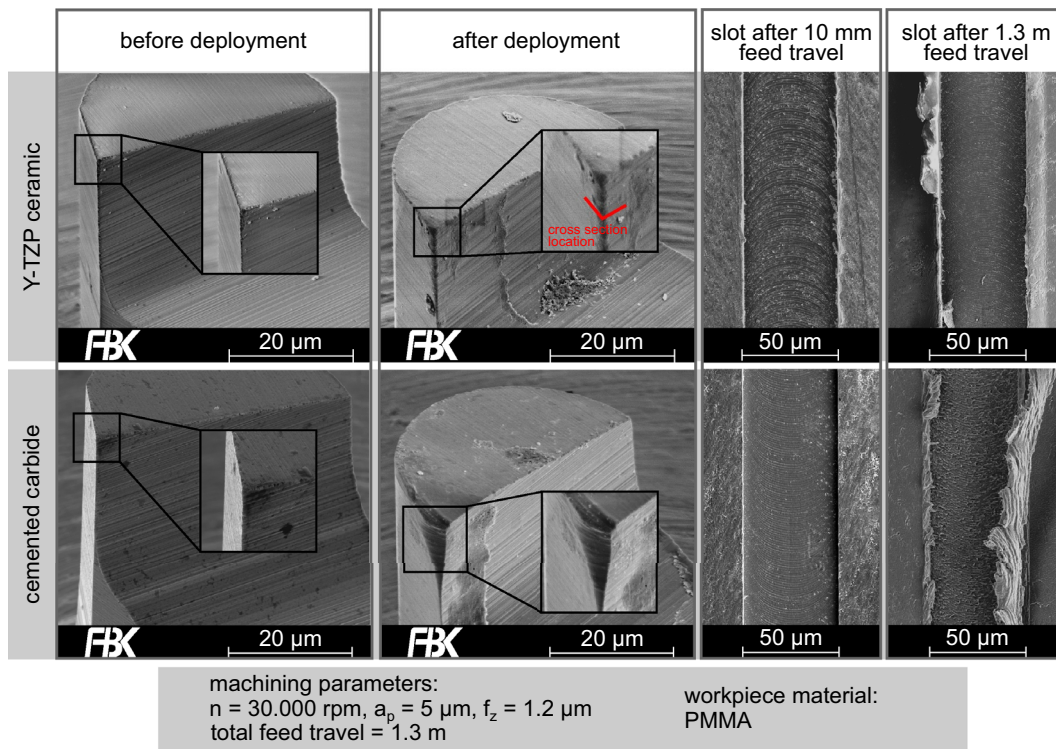


Fig. 9 Micro end mills and milled structures of the PMMA experiments

can be identified. Workpiece material adhesions are visible on the rake face for both tools. For the ceramic tool, less adhesions are present though, and they are further away from the cutting edge. The cemented carbide tool shows more adhesions in direct proximity to the cutting edge. The ‘wedge’ of the cemented carbide tool likely is a result of a locally washed-out cobalt phase due to adhesive wear, which then results in the WC-grains being exposed and pulled out by abrasion. The occurrence of the wear only at the flank face suggests that the chips are not removed via the rake face, but squeezed by the flank face under high pressure. With increasing wear, the wedge grows, and the actual cutting edge of the tool is moved inward to a lower effective cutting radius. This further increases the wear rate: The wedge area now is in direct contact with the workpiece material, as it is on the edge of the tool. As such, it is subjected to a high amount of friction.

For the milled slots, both tools show a high quality at the start of the feed travel, with little to no burr formation. Here, the slot milled with the cemented carbide tool is somewhat ‘clearer’, with less adhesions than the one milled with the ceramic tool. The milling kinematics are clearly visible for both, although for the cemented carbide tool they do not stretch towards the slot sides. This indicates that the minimum chip thickness was not reached at those locations. For the slot milled with the ceramic tool, the milling marks do extend to the slot sides. At the end of the feed travel, the slot milled with the ceramic tool is still of high quality, although the milling kinematics are not as clear as at the beginning. Burr formation has increased slightly, also. The slot milled with the cemented carbide tool however reflects the wear state of the tool at the end of the feed travel: Burr formation has increased, lots of adhesions are present, and the overall quality is lower.

To further analyze the tool wear, the cutting edge topographies measured with the AFM were used. Figure 10 shows one cross section of the cutting edge, 5 μm below the cutting edge corner (see indication in Fig. 9), for each of the two tools shown in Fig. 9.

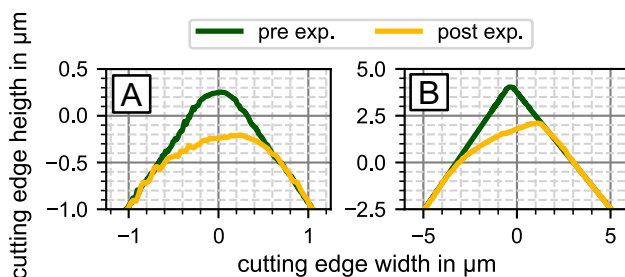


Fig. 10 Single cutting edge cross sections of the micro end mills deployed in PMMA, measured via AFM 5 μm from the cutting edge corner before and after the experiments: **A** Y-TZP ceramic tool, **B** cemented carbide tool

Figure 10A displays the cross section before and after machining for the ceramic tool. An increase in cutting edge radius can be observed (from 251 nm to 944 nm for the cross sections displayed), as was already evident from the SEM image. The wear is more pronounced on the flank face, though not as strong as the ‘wedge’ present for the cemented carbide tools. Relative to the cross sections of the cemented carbide tool before and after the experiment in Fig. 10B, however, the overall wear is minimal. The ‘wedge’ of the cemented carbide tool in Fig. 9 is immediately recognizable. The change in tool geometry from the new tool to the worn one is highlighted by the 5 \times larger scaling of the plot axes. The cutting edge radius rose from 236 nm to 3.35 μm . That value can be used as a reference only though, as the geometry after the experiment in B) can no longer be approximated by a radius.

The wear progress of the cemented carbide tools can be confirmed by the specific cutting forces, see Fig. 11. For the active force in Fig. 11A, a linear increase over the feed travel is observed for the cemented carbide tool, similar to previous studies [29].

This correlates with the wear process described above, the larger the wedge at the cutting edge corner, the more ploughing occurs. With the higher amount of friction the active force subsequently rises. The ceramic tools show active forces that remain mostly constant over the feed

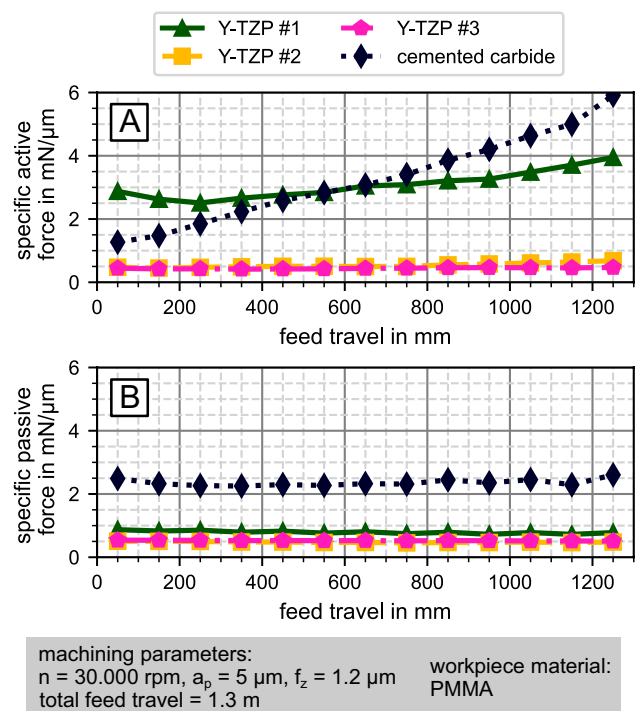


Fig. 11 Specific active (A) and passive (B) forces during micro milling of PMMA, mean forces over 100 mm feed travel, normalized with the slot depth as measured via confocal microscopy

travel, despite the increase in cutting edge radius measured above. Tool #1 is somewhat of an outlier, with higher force than both other ceramic tools, and slightly rising force level over the course of the feed travel. This could be due to a high runout from tool clamping, as a significantly altered cutting depth or friction between the tool's backside and the workpiece could explain this rise in force level. The passive forces in Fig. 11B on the other hand are constant over the feed travel for all tools, albeit they are much higher for the cemented carbide tool (about 3–4×). This concurs with the wear profile of the micro end mills in Fig. 9: Wear mainly occurs at the major cutting edge, and to a lesser degree at the minor cutting edge. Therefore, no or only slight additional friction occurs at the minor cutting edge/workpiece interface that would lead to increasing passive forces versus the feed travel.

Looking at the roughness values in Fig. 12 obtained from the confocal microscope, a very uniform progression is present for the ceramic end mills.

For both the profile and areal roughness in Fig. 12A, B, respectively, the values obtained from the slots milled with the ceramic tools are in the same range. No overall trend is visible with increasing feed travel, which is in line with the visual quality of the slot at the end of the feed travel in Fig. 9. The increase in cutting edge radius over the feed travel does not have an influence on the slot bottom quality, as the minor

cutting edge is not influenced by it. Yet, as with the visual tool wear and the active force, the cemented carbide tool shows a significant increase in surface roughness. Both Ra and Sa start with values as low as for the ceramic tools. They increase slightly until about 600 mm feed travel, but then rise to about twice their value. In contrast to the linear increase of the active force in Fig. 11A, it seems the tool wear has unproportionally more influence on the resulting surface quality the larger the 'wedge' at the cutting edge corner becomes. This could indicate that a certain amount of wear is required for the surface generation to be influenced by the resulting ploughing.

4 Discussion

Overall, the all-ceramic micro end mills were not able to achieve a similar performance increase versus cemented carbide tool substrates as in conventional machining. Especially for 1.7225 and 1.4404, the tool wear was severe in comparison to the cemented carbide tools. For both steels the wear occurred immediately, resulting in heavy ploughing and less actual material removal. This wear behavior is likely tied to the higher Young's modulus and/or hardness of steel, as the alumina alloy has similar tensile and yield strength to 1.4404. Typical ceramic tool materials in conventional machining are alumina or silicon nitride, which have higher hardness but lower fracture toughness than Y-TZP. These however suffer immediate breakages for tool diameters of 50 μm, likely due to the high local stresses and cyclic load rates in micro milling. With it's higher fracture toughness, Y-TZP can withstand these. However, it is not as wear resistant, likely due to the lower overall hardness.

Yet for PMMA, where cemented carbide tools show a wedge-like wear pattern, the Y-TZP tools only exhibit a slightly duller cutting edge. A possible explanation for this behavior could be that the cemented carbide tools are more susceptible to tribochemical wear than the all-ceramic ones. This could lead to individual cemented carbide grains breaking out of the bulk material, weakening the cutting edge further. The Y-TZP ceramic with its different microstructure is much more chemically inert than cemented carbide, which would result in the lower tool wear observed as no grains are breaking off. Regardless of the exact mechanism behind the high tool wear of cemented carbide tools, the tool wear is reduced significantly for all-ceramic micro end mills. As such, higher feed travels can be achieved, without the loss of structure quality. Also, the machining process is more stable, as the specific cutting force remain constant over the extent of feed travels tested in this study. This enables micro milling larger structures with higher aspect ratios,

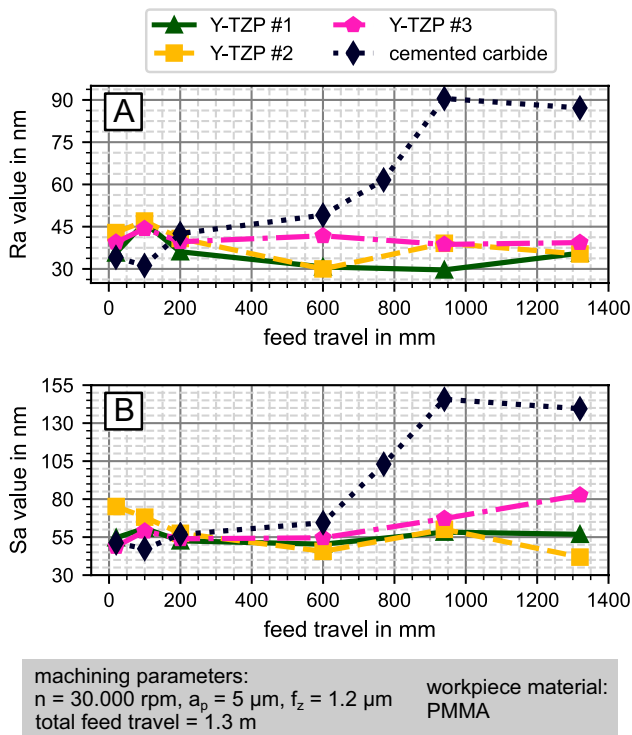


Fig. 12 Ra and Sa roughness values versus feed travel for the PMMA specimens

which would not be possible in with cemented carbide tools.

5 Conclusion

In this study, we deployed all-ceramic micro end mills made from Y-TZP in four different workpiece materials, to test whether we could transfer the positive wear aspects of ceramic tools from the macro processes down to the micro scale. For the two steels examined, the ceramic tools suffered severe wear, with entire parts of the minor cutting edge missing. Proper micro milled structures were only achieved for a few millimeters until the tool wear set in. For both steel materials, the cemented carbide tools used as reference showed less tool wear and higher quality structures, even at higher feed travels where the ceramic tools failed. For the aluminum alloy, the ceramic tools showed rounded cutting edge corners, slot geometries with angled sidewalls, and worse surface roughness than the cemented carbide tool. For these materials, the all-ceramic micro tools cannot be reasonably used and offer no improvement over cemented carbide tools. For the thermoplastic PMMA however, we have shown that significant improvements could be achieved by utilizing the Y-TZP ceramic tools: Less tool wear, lower and more stable cutting forces, and higher surface qualities. Therefore, higher feed travels can be achieved per tool, without sacrificing structure quality. As such, the positive wear aspects of ceramic tool substrates could be transferred from the macro level for micro milling of PMMA.

In further investigations, the influence of different Y-TZP substrates will be researched, along with varying process parameters when micro milling PMMA. Since the ceramic tools exhibit significantly lower tool wear than the cemented carbide ones, higher spindle speeds become available and will be researched, too.

Funding Open Access funding enabled and organized by Projekt DEAL. Funded by the Deutsche Forschungsgemeinschaft (DFG, German Research Foundation)—project number 407558930—associated project SFB926—project-ID 172116086.

Data availability Data will be made available on request.

Declarations

Conflict of interest The authors have no relevant financial or non-financial interests to disclose. ¹Naming of specific manufacturers is done solely for the sake of completeness and does not necessarily imply an endorsement of the named companies nor that the products are necessarily the best for the purpose.

Open Access This article is licensed under a Creative Commons Attribution 4.0 International License, which permits use, sharing, adaptation, distribution and reproduction in any medium or format, as long as you give appropriate credit to the original author(s) and the source, provide a link to the Creative Commons licence, and indicate if changes were made. The images or other third party material in this article are included in the article's Creative Commons licence, unless indicated otherwise in a credit line to the material. If material is not included in the article's Creative Commons licence and your intended use is not permitted by statutory regulation or exceeds the permitted use, you will need to obtain permission directly from the copyright holder. To view a copy of this licence, visit <http://creativecommons.org/licenses/by/4.0/>.

References

- Bang Y, Lee K, Oh S (2005) 5-axis micro milling machine for machining micro parts. *Int J Adv Manuf Technol* 25(9–10):888–894. <https://doi.org/10.1007/s00170-003-1950-1>
- Brunet A, Müller T, Scholz S (2017) *Mikrofertigungstechnologien und ihre Anwendungen—ein theoretischer und praktischer Leit-faden*. KIT Scientific Publishing, Karlsruhe
- Alting L, Kimura F, Hansen HN, Bissacco G (2003) Micro engineering. *CIRP Ann* 52(2):635–657. [https://doi.org/10.1016/S0007-8506\(07\)60208-X](https://doi.org/10.1016/S0007-8506(07)60208-X)
- Camara MA, Campos Rubio JC, Abrao AM, Davim JP (2012) State of the art on micromilling of materials, a review. *J Mater Sci Technol* 28(8):673–685. [https://doi.org/10.1016/S1005-0302\(12\)60115-7](https://doi.org/10.1016/S1005-0302(12)60115-7)
- Vollertsen F (2008) Categories of size effects. *Prod Eng* 2(4):377–383. <https://doi.org/10.1007/s11740-008-0127-z>
- Kirsch B, Bohley M, Arrabiyeh PA, Aurich JC (2017) Application of ultra-small micro grinding and micro milling tools: possibilities and limitations. *Micromachines* 8(9):261–279. <https://doi.org/10.3390/mi8090261>
- Cheng K, Huo D (2013) *Micro cutting*. Wiley, West Sussex
- Klocke F, Bergs T, Veselovac D, Arntz A, Quito FJ, Kratz S (2007) Von der Makro- zur Mikrowelt: Herausforderung für den Mikroformenbau. *wt Werkstattstechnik Online* 97(11/12):842–846
- Dornfeld D, Min S, Takeuchi Y (2006) Recent advances in mechanical micromilling. *CIRP Ann* 55(2):745–768
- Chae J, Park SS, Freiheit T (2006) Investigation of micro-cutting operations. *Int J Mach Tools Manuf* 46:313–332. <https://doi.org/10.1016/j.ijmactools.2005.05.015>
- García J, Collado Ciprés V, Blomqvist A, Kaplan B (2019) Cemented carbide microstructures: a review. *Int J Refract Metals Hard Mater* 80:40–68. <https://doi.org/10.1016/j.jrmhm.2018.12.004>
- Kieren-Ehse S, Mayer T, Kirsch B, Aurich JC (2021) Atomic force microscope for in situ micro end mill characterization—part I: integration into a desktop sized machine tool. In: *Proceedings of the 21st EUSPEN international conference*, pp 463–466
- Liu X, DeVor RE, Kapoor SG (2006) An analytical model for the prediction of minimum chip thickness in micromachining. *J Manuf Sci Eng* 128(2):474–481. <https://doi.org/10.1115/1.2162905>
- Balázs BZ, Geier N, Takács M, Davim JP (2021) A review on micro-milling: recent advances and future trends. *Int J Adv Manuf Technol* 112(3–4):655–684. <https://doi.org/10.1007/s00170-020-06445-w>
- Oliaei SNB, Karpat Y, Davim JP, Perveen A (2018) Micro tool design and fabrication: a review. *J Manuf Process* 36:496–519. <https://doi.org/10.1016/j.jmapro.2018.10.038>

16. O'Toole L, Fang FZ (2022) Optimal tool design in micro-milling of difficult-to-machine materials. *Adv Manuf.* <https://doi.org/10.1007/s40436-022-00418-w>
17. Fang FZ, Wu H, Liu XD, Liu YC, Ng ST (2003) Tool geometry study in micromachining. *J Micromech Microeng* 13:726–731
18. Hülsenberg D (2014) *Keramik: Wie ein alter Werkstoff hochmodern wird.* Springer, Berlin
19. Hao Z, Fan Y, Lin J, Ji F, Liu X (2017) New observations on wear mechanism of self-reinforced SiAlON ceramic tool in milling of Inconel 718. *Arch Civ Mech Eng* 17:467–474. <https://doi.org/10.1016/j.acme.2016.12.011>
20. Uhlmann E, Hübert C (2011) Tool grinding of end mill cutting tools made from high performance ceramics and cemented carbides. *CIRP Ann* 60:359–362. <https://doi.org/10.1016/j.cirp.2011.03.106>
21. Finkeldei D, Sexauer M, Bleicher F (2019) End milling of Inconel 718 using solid Si₃N₄ ceramic cutting tools. In: *Procedia CIRP* 81—Proceedings of the 52nd CIRP conference on manufacturing systems, vol 81, pp 1131–1135. <https://doi.org/10.1016/j.procir.2019.03.280>
22. Wang B, Liu Z (2016) Cutting performance of solid ceramic end milling tools in machining hardened AISI H13 steel. *Int J Refract Met Hard Mater* 55:24–32. <https://doi.org/10.1016/j.ijrmhm.2015.11.004>
23. Mayer T, Kieren-Ehse S, Kirsch B, Aurich JC (2022) Micro milling of brass and commercially pure titanium with all-ceramic micro end mills made from four different ceramic tool substrates. In: *Proceedings of the 22nd EUSPEN international conference*, pp 455–458
24. Heimann RB (2010) *Classic and advanced ceramics: from fundamentals to applications.* Wiley-VCH-Verl, Weinheim
25. Evans AG, Heuer AH (1980) Transformation toughening in ceramics: martensitic transformations in crack-tip stress fields. *J Am Ceram Soc* 63(5–6):241–248. <https://doi.org/10.1111/j.1151-2916.1980.tb10712.x>
26. Riedel R, Chen IW (2010) *Ceramics science and technology, vol 2: properties.* Wiley-VCH, Weinheim
27. Aurich JC, Reichenbach IG, Schüler GM (2012) Manufacture and application of ultra-small micro end mills. *CIRP Ann* 61(1):83–86. <https://doi.org/10.1016/j.cirp.2012.03.012>
28. Klauer K, Greco S, Kirsch B, Aurich JC (2021) Effect of vibration-assistance on tool wear, process forces and surface roughness when micro milling AISI 316L. In: *Proceedings of the 21st EUSPEN international conference*
29. Reichenbach IG, Bohley M, Sousa FJP, Aurich JC (2019) Tool-life criteria and wear behavior of single-edge ultra-small micro end mills. *Precis Eng* 55:55–58. <https://doi.org/10.1016/j.precisiong.2018.08.006>
30. DIN EN ISO 21920-2:2022-12 (2022) *Geometrische Produktspezifikation (GPS)—Oberflächenbeschaffenheit: Profile - Teil 2: Begriffe und Kenngrößen für die Oberflächenbeschaffenheit.* Deutsches Institut für Normung, Berlin. <https://doi.org/10.31030/3294016>
31. DIN EN ISO 4288:1998-04 (1998) *Geometrische Produktspezifikation (GPS)—Oberflächenbeschaffenheit: Tastschnittverfahren—Regeln und Verfahren für die Beurteilung der Oberflächenbeschaffenheit.* Deutsches Institut für Normung, Berlin. <https://doi.org/10.31030/7434013>
32. DIN EN ISO 25178-2:2012-09 (2012) *Geometrische Produktspezifikation (GPS)—Oberflächenbeschaffenheit: Flächenhaft - Teil 2: Begriffe und Oberflächen-Kenngrößen.* Deutsches Institut für Normung, Berlin. <https://doi.org/10.31030/1754208>

Publisher's Note Springer Nature remains neutral with regard to jurisdictional claims in published maps and institutional affiliations.